SSRG International Journal of Electrical and Electronics Engineering
ISSN: 2348-8379/ https://doi.org/10.14445/23488379/IJEEE-V11I12P138

Volume 11 Issue 11, 414-426, December 2024

Original Article

An Integrated Variational Decomposition Models for Overlapped Nonstationary Multicomponent Signal Isolation with Incomplete Data

Shaik Mohammed Shareef[1,*], M. Venu Gopala Rao[2]

[1,2]*Department of ECE, Koneru Lakshmaiah Education Foundation, Andhra Pradesh, India.*

[*]*Corresponding Author : skmohammedshareef7@gmail.com*

Received: 21 October 2024 Revised: 22 November 2024 Accepted: 20 December 2024 Published: 31 December 2024

Abstract *- Signal analysis is often challenging due to the complexity of signals, which comprise multiple components that can overlap in frequency and be affected by noise and interference. In many cases, only partial information about these components is available, making signal analysis even more difficult. This paper presents a method to decompose such complex signals using Integrated Variational Decomposition Models. The procedure begins with generating a partially completed multicomponent signal based on radar equations. Then, the signal is transformed into a time-frequency representation using the Short-time Fourier Transform (STFT). Then, a technique called compressive sensing, specifically Rapid Iterative Shrinkage Thresholding Network (RISTN), is utilized to restructure the time-frequency representation by solving a sparse regularization problem. The Instantaneous Frequencies (IF) are subsequently estimated using the Simplified Variational Mode Decomposition (SVMD) algorithm. Finally, the individual components of the overlapped nonstationary multicomponent signal are isolated using an algorithm called Extended Variational Chirp Component Decomposition (EVCCD). The proposed method outperforms existing methods in terms of Root Mean Square Error (RMsE), Mean Squared Error (MSE), Root Mean Absolute Error (RMAE), and computational time, achieving better values such as -15.829 dB, -31.062 dB, 0.034 dB, and 0.90282 respectively.*

Keywords *- Compressive sensing, EVCCD, Integrated variational decomposition models, Multicomponent signal, Non-stationary signal, Radar equations, RISTN, STFT, Signal analysis, SVMD, Time-frequency representation, Variational decomposition.*

1. Introduction

The micro-Doppler (m-D) effect is a phenomenon observed when a target or its structures exhibit micro-motion dynamics such as vibration, rotation, or bulk translation. These dynamics result in frequency modulation, producing time-varying sidebands around the target's Doppler frequency. This effect is significant in radar signal processing, providing valuable information about the target's movement and characteristics. Typically, multicomponent m-D signals are echoes from multiple micromotion targets or various micromotion sections of a single target [1-3].

The challenge arises when overlapping components contain multiple m-D signatures from different parts or targets, making the decomposition of multicomponent m-D signals a compelling research area. For instance, swaying a person's limbs or the rotational frequencies of different space targets illustrate such micromotion parts and targets.

Nonparametric techniques are favoured over parametric ones due to their time efficiency and robustness in extracting m-D signatures. These techniques rely on the Time-Frequency Representation (TFR) of signals, making the understanding of micromotion features in the TF domain crucial for the success of TFR-based approaches. However, two main issues hinder the practical extraction of micromotion features: 1) m-D component signal overlap and 2) incomplete radar echo sampling [5, 6].

Incomplete data can result from random corruption or removal of samples due to radar malfunctions or severe interference. When different micromotion components of a target are packed into one range cell or a cluster of similar range cells, their multicomponent m-D signals overlap or cross in the TF domain.

Sparse signal processing methods based on compressive sensing have been suggested to address the challenges posed by micromotion targets, including denoising and reconstruction of incomplete or distorted data. These methods primarily focus on TFR reconstruction rather than decomposing multicomponent m-D signals [1, 7, 8].

Yet, decomposing multicomponent m-D signals can reveal extensive information about various micromotion targets. The m-D signal, being a type of cyclostationary signal, works well with nonstationary signal processing approaches. To implement various multicomponent nonstationary signal decomposition methods such as Adaptive Chirp Mode Pursuit (ACMP), Variational Nonlinear Chirp Mode Decomposition (VNCMD), and Variational Modal Decomposition (VMD), it is essential to maintain separation or non-overlapping of multicomponent in the TF domain. Several studies have proposed this requirement [9-13].

The Ridge Path Regrouping (RPRG) technique successfully separated overlapping m-D signals in the TF domain for regular modulation. Thus, the Short Temporal Variational Mode Decomposition (STVMD) method is effective for accurately decomposing overlapping m-D signals with irregular modulation in the Instantaneous Frequency (IF) domain. For multicomponent m-D signal decomposition, signal separation approaches based on the timescale-chirp rate operator, Fractional Fourier Transform (FFT), and chirplet transform have been utilized. However, these techniques depend on complete m-D signal samples with multiple components. Consequently, the goal of TFR reconstruction using partial data is to use the incomplete data to extract multicomponent m-D signals.

Xin Huang et al. [18] proposed a multicomponent collaborative time-frequency state-space method to decompose vibration signals. The technique used a multicomponent proportional model to accurately specify the synchronization of high-frequency and rotating-frequency components. This structure allowed for the precise dissection of multicomponent vibration signals in scenes with varying speeds by feeding the IF change curves of various components into the Vold-Kalman filter technique. Experimental findings showed this technique effectively achieved precise IF tracking and signal decomposition. However, the model's assumptions and sensitivity to noise limited accurate vibration signal decomposition, particularly in complex scenarios.

Empirical Mode Decomposition (EMD) has been suggested by Quentin Legros et al. [3] as a method for estimating IF and amplitude in multicomponent signals. The primary goal of this algorithm was to address the challenge of evaluating the modes' IF and amplitude in the presence of noise in nonstationary multicomponent signals. In a Bayesian structure, a new observation model was created for the signal spectrogram to manage complex configurations with overlapping elements or noise. An expectation-maximization approach with stochastic variations was employed to estimate the model parameters. The outcomes showed that this algorithm reduced the complexity of the problem and used acceptable computational time to assess mixture weights. However, the algorithm would need to expand the approach for chirp rate estimation and generalization for hyperparameter estimation.

Jamal Akram et al. [19] proposed a new method for estimating the IF of multicomponent signals in the time-frequency domain based on crossing signatures. This technique recursively determined the IFs of the signal components using time-frequency filtering and Eigen decomposition of time-frequency distributions to separate them from the original mixture. Experimental results proved this method was better, but nonstationary and cross-component interference made it challenging to correctly separate the signal components. Additionally, computational complexity issues hindered real-time applications and limited feasibility.

Lu Yan et al. [20] introduced a mechanically variable nonstationary signal separation approach based on IF estimation. The objective was to achieve a densely concentrated time-frequency energy using Multi-Scale Chirp Sparse Representation (MSCSR) for IF identification, extraction, and Trending. An adaptive time-varying filter was constructed using the recovered Intermediate Frequency (IF) to separate the nonstationary fast signal. A rapid IF fluctuation experiment validated the efficacy of this approach for robust time-varying signals, showing it could effectively extract rapid oscillation IF with an error of less than 10%. However, the approach had limitations such as low computational performance, limited noise resistance, and reduced accuracy.

Lei Tang et al. [21] introduced an LMSST with Adaptive Window Width (AWW) to identify time-varying structures at instantaneous frequencies. Combining a window width optimization algorithm and autoregressive power spectrum-based variational modal decomposition (AR-VMD), an adaptive technique was formed to calculate the window width of ALMSST. The AR-VMD broke down the complex signal into its constituent parts, and the window width optimization technique used the Renyi entropy as an evaluation index to choose the optimal window width for each mono-component signal. Simulation and experimental results showed that ALMSST effectively found the IFs of structures that change over time. However, spectral leakage and windowing artifacts could hinder the reliable recognition of IFs in nonstationary signals.

Existing techniques for decomposing multicomponent micro-Doppler signals face several concerns, making it challenging to handle overlapping signals and incomplete data. Handling complex signals with crossing fingerprints is difficult because multicomponents must be either non-overlapping or physically separated in the time-frequency domain. Techniques include Adaptive Chirp Mode Pursuit (ACMP) and synchro-squeezed wavelet transform.

SST are vulnerable to noise and inaccurate Time-Frequency Representations (TFRs) when dealing with partial data. These limitations make it challenging to correctly decompose multicomponent micro-Doppler signals, especially when incomplete data samples or signals overlap. Additionally, current methods for deriving micromotion characteristics from TFRs can be hindered by the signal overlapping of micro-Doppler components and inadequate radar echo sampling. Both nonparametric and parametric approaches struggle with incomplete data samples, which may be corrupted or missing due to interference or radar failures.

The problem of signal overlapping in the time-frequency domain further complicates the decomposition process, resulting in overlapping signals that are difficult to differentiate using conventional approaches. These limitations highlight the need for sophisticated decomposition techniques to handle the complexity of multicomponent micro-Doppler signals with incomplete and overlapping components. The major objectives of the proposed work are:

1. To introduce a novel method for multicomponent signal decomposition using Integrated Variational Decomposition Models.
2. To offer a compressive sensing approach to address the sparse regularization problem for TFR reconstruction.
3. Using an Extended Chirp Component Decomposition algorithm to isolate the individual components of overlapped nonstationary multicomponent signals.
4. To compare the experimental outcomes with existing methods to determine the superiority of the proposed work.

The residual content of the paper is organized as follows: Section 2 describes the proposed model in detail. Section 3 examines the overall performance of the proposed model with existing techniques discussed with graphs. Finally, the complete conclusion of the proposed model is presented in Section.

2. Proposed Methodology

Signals are often multicomponent in practice, meaning they may be expressed as linear combinations of separate signals (components). Multicomponent signals consist of overlapping components where the frequency ranges of various components may intersect. Also, they are susceptible to noise and interference from various sources. In addition, they may be sparse or incomplete, meaning that only partial information about the signal components is available. As a result, it is difficult to decompose multicomponent signals when dealing with incomplete and noisy data. Using Integrated Variational Decomposition Models, this research will present a method for multicomponent signal decomposition, which will address this issue. Figure 1 displays the proposed methodology workflow.

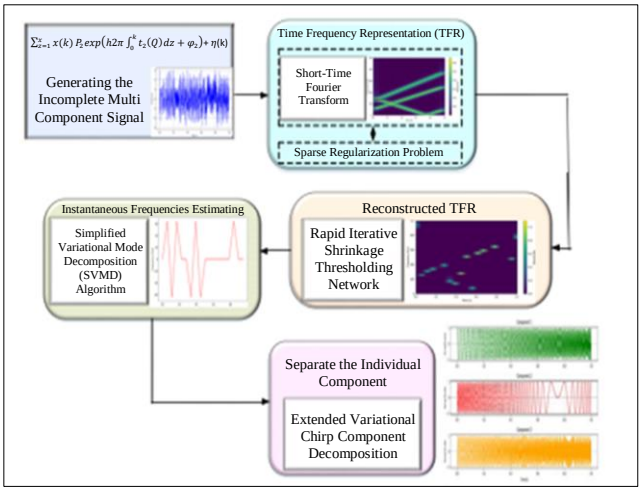

Fig. 1 Architecture for proposed work

Here, the incomplete multicomponent signal will be initially generated using the narrowband radar equations from a micromotion target. After that, the STFT will be used to obtain the TFR of the input signal. After that, a sparse regularization problem will be formulated for TFR reconstruction. This problem will be solved using a compressive sensing approach, namely, RISTN. After the reconstruction of TFR, the IF will be estimated using the SVMD algorithm. After estimating the IF, the individual component of the overlapped nonstationary multicomponent signal will be isolated by introducing an EVCCD algorithm. The above-described technique is detailed below.

2.1. Signal Generation Mode

The point-scattering model is an appropriate match for the fake metal targets and high-frequency electromagnetic settings. Due to imperfect sampling, a micromotion target is formed from the multicomponent signal received by a narrowband radar. Figure 6 shows the result of the following mathematical expression for this signal.

$$G(k) = \sum_{s=1}^{x} G_s(k) + \eta(k) \tag{1}$$

$$= \sum_{s=1}^{x} x(k)\, p_s(k) \exp\left(h2\pi \int_0^k t_s(G)ds + \varphi_s \right) + \eta(k) \tag{2}$$

Here, the variable x represents the number of components, which has been defined earlier in the letter. The symbol x(k) denotes the available sampling while $x(k) \subset \{0,1\}$,$p_s(k)$ representing each scattering point's instantaneous amplitude. The term $p_s(k)>0;\varphi_s$ mentioned for the initial phase and $t_s(t)$ is the IF. Lastly, $\eta(k)$ characterizes the additive noise. The instantaneous amplitude $x(k) \subset \{0,1\}$,ps(k) and intermediate frequency $t_s(t)$ are smooth and slowly varying functions, which implies that they change gradually over time.

These functions satisfy the condition,

$$|p'_s(k)|, |t'_s(k)| << |t_s(k)|$$

Where, $<<$ is a small positive constant.

2.2. STFT Using TFR

Because of its linearity, the STFT is a popular TFR technique for micromotion modulation, even though G(k) is a nonstationary signal. The STFT of echo G(k) can be exemplified as:

$$STFT(k,t) = \int G(t) R\sigma(k-\tau) \exp(-h2\pi t\, k) dt \quad (3)$$

Here, Rσ indicates the window function, which has two possible expressions: a Hamming window and a Gaussian window, is used in this symbol. The window's length is represented by the symbol σ, which ensures that the windowed signals are adequately stationary.

The STFT of the signal with missing data can be defined using the matrix formulation below:

$$E^0_{(IJ)\times 1} = \psi_{(I\,J)\times(I\,J)} C_{(I\,J)\times I} D_{I\times I}\, g^0{}_{I\times 1} \quad (4)$$

Here, the matrix of Fourier transform is represented as $\psi = diag\{\phi,..., \phi\}$ and ϕ; $I = Jjg$, j_g is denoted as the time step; and j_g=1; $C = [W_1,....W_j,....W_J]^B$ is the sliding Gaussian window, where, $W_j = diag\{w^j(1),....., w^j(i),...w^j(I)\}$ and $i \in [1, I]$; $D = diag\{d(1),..., d(i),...d(I)\}$ is the imperfect sampling matrix, $d(i) \in \{0,1\}$; g^0 is the optimal signal that contains all the necessary information, $g^0 = [g^0(1),..., g^0(i),...g^0(I)]^B$; $(\bullet)^B$ is denoted as the transpose, and $diag\{\bullet\}$ is denoted as the diagonalization operator.

Effective techniques exist for estimating IFs. Nevertheless, the effectiveness of these techniques depends on the TFR's caliber. Because of the lack of data, the TFR was defocused, denoted by E^0. Denoising and reconstructing the well-focused TFR can be achieved by modeling the signal with partial data g using,

$$g = DF_E + i \quad (5)$$

Here $g = [g(1),...g(i),...g(I)]^B$; F is denoted as the pseudo-inverse of ψC; and i is additive noise vector; $i = [\eta(1),...\eta(i),...\eta(I)]^B$. The entire information of TFR is mentioned as. In order to extract g from partially sampled data, (5) can be thought of as an optimization issue.

$$\hat{E} = \arg\min_E \|g - DF_E\|_2^2 \quad (6)$$

Typically, there are only a certain number of strong scatters dispersed around the target. Here is a different way to rewrite the optimization model from (6) using these spars prior:

$$\hat{E} = \arg\min_E \|g - DF_E\|_2^2 + \lambda \|E\|_d \quad (7)$$

Here, $0 \le d \le 1$, $\|E\|_d$ are regularization terms; the regularization parameter, λ>0, has the ability to balance the two-goal terms. Given the optimization model in eqn. (7) since $0 \le d \le 1$, the v_1-norm has the best convex approximation, it becomes,

$$\hat{E} = \arg\min_E \|g - DF_E\|_2^2 + \lambda \|E\|_1 \quad (8)$$

The regularization-related Equation (8) can be rewritten as a linear programming issue. Finally, the STFT generate the TFR signal, and its output is shown in Figure 7.

2.3. Sparse Regularization Problem Optimized Using RISTN

The sparse regularization problem can be efficiently solved by the RISTN method. The proposed RISTN to solve the (8) is formulated as:

$$p^{(k)} = u^{(k)} - (G^{(k)})^B (Wu^{(k)} - r) \quad (9)$$

$$E^{(k)} = \tau_{\theta(k)}(p^{(k)}) \quad (10)$$

$$u^{(k+1)} = E^{(k)} + \rho^{(k)}(E^{(k)} - E^{(k-1)}) \quad (11)$$

Here, it represents the intermediate variables of the outcome $p^{(k)}$, $u^{(k+1)}$, and $E^{(k)}$; $G^{(k)}$ is denoted as the gradient operator, $\tau_{\theta(k)}$ stands for the proximal nonlinear operator, $\rho^{(k)}$ is identified as the momentum update scalar.

By utilizing a trained network as a proximal operator in (10), RISTN minimizes the non-differentiable section, and by utilizing gradient information in (9), it minimizes the smooth differentiable part. The previous two iterations are combined in a two-step linear fashion to create the update (11).

The RISTA net detail is described in the following, and the RISTN model includes the three models: gradient descent model $p^{(k)}$, proximal mapping module $E^{(k)}$, and momentum module $u^{(k+1)}$.

2.3.1. Gradient Descent Module $p^{(k)}$

Since the preceding layer's output was $u^{(k)}$, this layer updates the reconstructed TFR using the gradient descent operation of Equation (9), which is the closed-form numerical solution to the data consistency subproblem. Specifically, it seeks to decrease $\|Wu - r\|_2^2$ by finding a more precise estimate. Because the physical model is associated with the data consistency term, it stabilizes the solution by imposing a physical constraint. The theoretical discussion focuses on learning with a well-established forward operator, which has the potential to reduce the maximum error bounds.

When dealing with situations involving Gaussian noises, the Equation of (9), when let $G^{(k)} = \mu W$ be a vector with $Z(E) = \|E\|_1$, simplifies to. The RISTA was motivated by ISTA and suggested that, instead of establishing the matrices' weights, ISTA should learn them:

$$E^{(k+1)} = \tau_\alpha \left(G_1^{(k)} r + G_2^{(k)} E^{(k)} \right) \quad (12)$$

For RISTA convergence to take place, it must be:

$$G_2^{(k)} - (F - G_1^{(k)}) \to 0, \qquad as\, k \to \infty \quad (13)$$

By allowing $G_1^{(k)} = (G^{(k)})^B$, $G_2^{(k)} = F - G^{(k)} W$ it to converge, Equation (9) meets the required condition. The weight $G^{(k)}$ in Equation (9) is a linear operator with the same dimensions as $G^{(k)}$. It may be expressed as the multiplication of a scalar $\mu^{(k)}$ and a matrix $\overset{\rho}{G}$, which is autonomous of the layer index k.

$$G^{(k)} = \mu^{(k)} \overset{\rho}{G} \quad (14)$$

Here, $\overset{\omega}{G}$ is denoted as the small consistency with W. The matrix $\overset{\rho}{G}$ is constructed in advance by explaining:

$$\overset{\rho}{G} \in \arg\min \left\| G^B W \right\|_T^2 \quad (15)$$

Minimizing the Frobenius norm of $G^B W$ under-linear restrictions is the goal of Equation (12). This is an easy-to-solve standard convex quadratic program. After $\overset{\rho}{G}$ is solved beforehand, end-to-end training is used to determine step size $\mu^{(k)}$.

2.3.2. Proximal Mapping Module $E^{(k)}$

When applied to an intermediate result $p^{(k)}$, the proximal operator's thresholding in a certain transform domain attempt to eliminate artifacts and noise. To capture complicated TFR characteristics in practice, the current sparse transformation needs to be fine-tuned. RISTN aim to acquire an extra stretchy demonstration $\tau(\cdot)$ and threshold $\theta^{(k)}$ from training data.

A RISTN $\tau(\cdot)$ is a four-linear convolutional operator with a ReLU in the middle. X_o filters, measuring 3 x 3, are represented by the first convolutional operator, whereas X_o filters, measuring 3 x 3 x X_o, are represented by the remaining three convolutional layers. It is assumed that $X_o = 32$ is the default. The advantages of residual learning can be inherited by establishing a skip connection from the input to the output. Recent research has shown that batch-normalizing layers are increasingly prone to introducing undesirable artifacts as the network gets deeper and more complex, which is why batch normalization is not used.

The sparse transform is invertible mathematically, or $\tilde{M} \circ M = \mathrm{N}$, where N is the uniqueness operator. Motivated by the sparse auto encoder's loss utility, which defines the transform $M(\cdot)$ loss as,

$$\begin{aligned} Y_{tsf} &= \lambda_1 Y_{sym} + \lambda_2 Y_{spa} \\ &= \lambda_1 \sum_{k=1}^{c_s} \left\| \tilde{M}\left(M\left(P^{(k)} \right) \right) - P^{(k)} \right\|_2^2 + \lambda_2 \sum_{k=1}^{c_s} \left\| M\left(P^{(k)} \right) \right\|_1 \end{aligned} \quad (16)$$

Where Y_{sym} represents a lack of regularity in inversion, while Y_{spa} represents a constraint that is not densely populated. In the RISTA-Net, the parameters $\tau(\cdot)$ are shared across iterations, but $\theta^{(k)}$ the value used for shrinkage thresholding is a parameter that can be learned.

Due to the changing variance of noise and artifact over the iterations, the variable $\theta^{(k)}$ is permitted to change at each level of the cascade.

2.3.3. Momentum Module $u^{(k+1)}$

The original ISTN can be made faster by adding a momentum term, just like RISTN, which converges in function values $A(1/k^2)$ at a faster pace than $A(1/k^2)$ ISTN. The faster convergence rate of the method compared to ISTA is due to its intelligent selection of update weights for the two prior findings, eliminating the need for further gradient evaluation.

In RISTN, this benefit is achieved by adjusting the persistent update weights $\{z^{(k)}\}$ of Equation (11) using a learnable parameter $p^{(k)}$, which is automatically cultured from the training dataset.

The loss utility for RISTN is defined as:

$$E_{total} = E_{mse} + \lambda_1 E_{sym} + \lambda_2 E_{spa} \quad (17)$$

The variable E_{mse} represents the MSE loss between the projected yield of RISTN and the crushed truth IFs. Lastly, train the network with a consistent set of hyperparameters for various tasks. The value λ_2 is reduced since the thresholding algorithm produces a comparable outcome. Finally, the RISTN model solves the sparse regularization problem in TFR reconstruction.

2.4. SVMD Using IF

Following the reconstruction of TFR, IF estimation is executed using the SVMD technique. In cases where IFs do not intersect, the traditional SVMD approach is still applicable. However, in the TFR domain, most multicomponent signals exhibit overlap.

To overcome this, a modified SVMD approach, integrating IF tracking and regrouping, is suggested. In SVMD, VMD is introduced to derive Intrinsic Mode Functions (IMF) and frequencies from the stable window signal of STFT. The IMF and frequencies are subsequently monitored and reassembled utilizing the Kalman filter for Intermediate Frequency (IF).

In the TFR domain, the location and speed of IF are described by the linear state space model. For simplification purposes, a one-dimensional constant velocity chosen

$$\hat{E}(k) = \begin{bmatrix} T_{k,s} \\ T_{k,s} \end{bmatrix} \quad (18)$$

$$\hat{E}(k) = \begin{bmatrix} 1 & Rs \\ 0 & 1 \end{bmatrix} \hat{E}_{k-1} + T_{k-1} \quad (19)$$

$$w_k = \begin{bmatrix} 1 & 0 \end{bmatrix} \hat{E}_k + m_k \quad (20)$$

Here, $T_{k,s}$ is denoted as the velocity, $R_s = 1/v_c$, the sampling frequency is denoted as v_c, with a measurement represented as w.

$T \sim I(0, P)$, $m \sim I(0, q)$ is denotes the process and measurement noise respectively, with P as the process covariance and the covariance of the noise observation is mentioned as q.

At intersections, a Kalman filter is used to anticipate the condition of the following frame in order to prevent Identification (ID) switching. The initial center frequency setting does affect the SVMD outcome, which is a relief. The decomposition result aligns with the starting value, facilitating IF tracking and regrouping and accelerating algorithm convergence.

This is achieved by pre-setting the next time's initial value according to the Kalman filter's prediction result. In particular, the algorithm's validity is greatly affected by the estimation of the filtering parameters p and q.

Similar to VMD, the SVMD method takes α the punishment parameter, ρ the scaling factor for updating the Lagrangian multipliers, S the number of modes, and the tolerance of the stop conditions as input parameters. The purpose of this study is not to address all the parameters; nevertheless, some of these parameters are associated with the ADMM solver; for more information on these parameters [16].

For example, the study requires that the number S be manually fixed before it can be used. The two most crucial parameters in the SVMD method are α and ρ. Along with the augmented Lagrangian technique for signal decomposition from overlapping sources, the anticipated center frequencies act as a priori knowledge. The window signal can be expressed as the Fourier transform operator applied to a reshaped matrix,

$$E^k = DTFT^p \{\mathrm{Re}\, shape(y, H, H)\} \quad (21)$$

Here, $DTFT^p\{.\}$ is denoted as the Fourier transform operator, and redesign (U, m, n) is a $m \times n$ matrix whose elements are taken column-wise form U. Figure 9 displays the results, while Table 1 shows the initialization of the IFs and the TFR reconstruction.

Table 1. TFR reconstruction and IFs initialization

Initialization $u^{(1)} = 0$, $k = 0$

While $\dfrac{\left\| \hat{u}(k) - \hat{u}^{(k-1)} \right\|_2^2}{\left\| \hat{u}(k-1) \right\|_2^2} > \xi$ do

$$k = k+1, u^{(k+1)} = u^{(k)} + \rho^{(k)}(E^{(k)} - E^{(k-1)})$$

End while

Obtained window signal via in-equation

$$E^k = DTFT^p \{\mathrm{Re}\, shape(y, H, H)\}$$

Input E^k to SVMD method

Obtained initial IF_S by SVMD method

2.5. Individual Component Signal Decomposition

After estimating the IF, the individual component of the overlapped nonstationary multicomponent signal will isolated by introducing an EVCCD algorithm. Afterwards, an optimization model is created and used to reconstruct the complex envelope using ADMM because it has a smooth prior and shows sparsity in the time-frequency domain.

Furthermore, the phase error is estimated using the least-square error criterion. A low-pass filtering operator is used to smooth down the IF estimation error generated by unwrapping the phase ambiguity operator. The problem of iterative optimization can be expressed as follows.

$$\min_{R_k,\overline{G}_k,L_k} \left\| R_k^p - A\widetilde{G}_k \overline{G}_k^p L_k^p \right\|_2^2 \qquad s.t \quad R = \sum_{k=1}^{x} R_k^p \qquad (22)$$

Here, p is denoted as the repetition counter, R_k is denoted as the separate constituent; the complex envelope,

$$L_k = [\overline{m}_k(1),.....\overline{m}_k(i),....., \overline{m}_k(I)]^G$$

Where,

$\overline{m}_k(i) = m_k \exp(\varphi k)$ $\overline{G}_k^p = diag\left\{\exp(h2\pi \sum_{t=1}^{i} \Delta w_k^{-h}(t))\right\}$ is the phase error; Δw_k^{-h} is the IF error; and the phase of initialization $\widetilde{G}_k = diag\left\{\exp(h2\pi \sum_{t=1}^{i} \Delta w_K(t))\right\}$.

The EVCCD method is presented to remove R_k^p; the complex envelop L_k^p can be demonstrated by Fourier series; and

$$L_k^p = SN_k^p$$

Where,

$N_k = \left[m_0^{(k)},...., m_t^{(k)},....m_T^{(k)} n_1^{(k)},..., n_t^{(k)},....n_T^{(k)}\right]^B$ are the Fourier coefficients, and the element configuration $S \in C^{I\times(2T+1)}$ can be designated as below:

$$(S)_{id} = \begin{cases} \cos[2(d-1)\pi w_0 z_i & d \in [1, T+1] \\ \sin[2(d-T-1]\pi w_0 z_i & d \in [T+2, 2T+1] \end{cases} \qquad (23)$$

Here, $w_0 = W_{R/}FI$, W_R is the sampling rate, $F \in \mathrm{I}^*$, and F=2. A time-frequency filter bank, abbreviated as Iw_0, is fundamental to the EVCCD technique. Modifying the optimization function in Equation (22) looks like this:

$$\min_N \left\| R - W^p N^P \right\|_2^2 + \nu \left\| N^P \right\|_2^2 \qquad (24)$$

Here,

$W^p = [W_1^p,....., W_k^p,...W_q^p], W_k^p = A\widetilde{G}_k \overline{G}_k^p S,$

$N^p = [N_1^p,....N_k^P,...N_q^p]^B$, and $\lambda_2 > 0$ is a weighting factor. The answer to Equation (24) is as follows, using the Tikhonov regularization method:

$$N^P = \left((W^P)^J W^P + \nu C\right)^{-1} (W^p)^J R \qquad (25)$$

Here, J is denoted as the identity matrix. The following is an expression for the individual component signal:

$$R_k^p = W_k^p N_k^p = A\widetilde{G}_k \overline{G}_k^p S N_k^p \qquad (26)$$

In the end, EVCCD yields the individual component R_k^p. Equation (22)'s optimization function can be rewritten as follows because the complex envelope L_k has a smooth prior and is sparse in the time-frequency domain.

$$L_k^{(p+1)} = \arg\min_{L_k} \frac{1}{2} \left\| R_k^p - A\widetilde{G}_k \overline{G}_k^p L_k^p \right\|_2^2 + \sigma \left\| \overline{O} L_k^P \right\|_1 + \frac{e}{2} \left\| \Omega L_k^p \right\|_2^2 \qquad (27)$$

In this case, $\overline{O} = \psi X$ and Ω are two distinct matrices of second order; the fidelity term is represented by the first term, while the restrictions on $\overline{O}L_k$ and L_k, sparse and smoothness, are imposed, respectively, by the second and third terms. The issue given in Equation (27) can be reformulated in ADMM by performing the operation of variable splitting; this process then repeats the following three phases;

$$W_k^{-y} = soft\left(\overline{O} L_k^{(y)} + e^{(y)}, \frac{\sigma}{\rho}\right) \qquad (28)$$

$$L_k^{(y+1)} = \left((A\widetilde{G}_K \overline{G}_K^P)^J (A\widetilde{G}_K \widetilde{G}_K^P) + \rho \overline{O}^J \overline{O} + ...e(\Omega)^j(\Omega)\right)^{-1} \times \left((A\widetilde{G}_K \overline{G}_K^P)^J R_K^P + \rho \overline{O}^J (w_k^{-(y)} - e^{(y)})\right) \qquad (29)$$

$$e^{(y+1)} = e^{(y)} + \overline{O} L_k^{(y+1)} - w_k^{-(y)} \qquad (30)$$

With the stopping criterion,

$$\left\| L_k^{(y+1)} - L_k^{(y)} \right\|_2^2 \Big/ \left\| L_k^{(y+1)} \right\|_2^2 < \gamma \qquad (31)$$

Here, y stands for the ADMM iteration counter, γ for a relative error, ρ for the update parameter, and e, as a whole, for the residuals throughout time. Ultimately, ADMM yields the intricate envelope $L_k^{(p+1)}$.

In order to estimate the phase error, since $\overline{G}_k$ is unfamiliar, designate a least-square-error model.

$$\overline{G}_k^{(p+1)} = \arg\min_{G_k^{-y}} \left\| R_k^p - \tilde{G}_k \overline{G}_k^p L_k^{(p+1)} \right\|_2^2 \quad (32)$$

Here, $\overline{G}_k = diag\{\exp(y\theta(I))\}$; the issue raised by (22) can be rephrased as follows:

$$\left\| R_k^p(i) - \exp(y\theta(i)) \tilde{G}_K L_K^{(P+1)} \right\|_2^2 = \left\| R_K^P(i) \right\|^2 + \left\| \tilde{G}_K L_K^{(P+1)} \right\|^2 - N - N^J \quad (33)$$

Here, $N = \exp(y\theta(i))(R_k(i))^J \tilde{G}_k L_k^{(p+1)}$ is a complex-valued scalar and $\theta(i)$ satisfies,

$$\theta_k(i) = a\tan\left(\frac{\mathrm{Im}\left(R_k(i) \left(\tilde{G}_k L_k^{(p+1)} \right)^J \right)}{\mathrm{Re}\left(R_k(i) \left(\tilde{G}_k L_k^{(p+1)} \right)^J \right)} \right) \quad (34)$$

The following is an expression for the IF increment:

$$\Delta W_k = \frac{1}{2\pi} \frac{d(unwrap(\theta_k))}{dt} \quad (35)$$

Where the unwrapping phase ambiguity operator is represented by the letter $unwrap(\cdot)$. The IF estimate error is smoothed using the low-pass filtering operator to lessen the impact of noise.

$$\min_{\Delta w_k^{-(p+1)}} \left\| \Delta w_k^{-(p+1)} - \Delta w_k \right\|_2^2 + \mu \left\| \Omega \Delta w_k^{-(p+1)} \right\|_2^2 \quad (36)$$

The solution of (31) is,

$$\Delta w_k^{-(p+1)} = (P + \mu \Omega^J \Omega)^{-1} \Delta w_k \quad (37)$$

Lastly, (32) yields the IF estimation error. Table 2 describes the individual component decomposition technique, and Figure 10 displays the results of the EVCCD algorithm.

Table 2. Decomposing components one by one

Input relative error ν, γ, parameters $\nu, \sigma, e, \rho, \mu$, $p = 0$

While $\left\| R_k^{(p)} - R_k^{(p-1)} \right\|_2^2 / \left\| R_k^{(p-1)} \right\|_2^2 > \nu$ do

$p = p+1,\ W_k^p = A\tilde{G}_k \overline{G}_k^p S$

$N^P = \left((W^P)^J W^P + \nu C \right)^{-1} (W^P)^J R$

$R_k^p = W_k^p N_k^p = A\tilde{G}_k \overline{G}_k^p S N_k^p$, Set $J = 0$

While $\left\| L_k^{(y+1)} - L_k^{(y)} \right\|_2^2 \Big/ \left\| L_k^{(y+1)} \right\|_2^2 < \gamma$ do

$J = J+1\ W_k^{-y} = soft\left(\overline{O} L_k^{(y)} + e^{(y)}, \frac{\sigma}{\rho} \right)$

$L_k^{(y+1)} = \left((A\tilde{G}_k \overline{G}_k^p)^J (A\tilde{G}_k \overline{G}_k^p) + \rho \overline{O}^J \overline{O} + \ldots\ldots e(\Omega)^J(\Omega) \right)^{-1} \times \left((A\tilde{G}_k \overline{G}_k^p)^J R_k^p + \rho \overline{O}^J (w_k^{-(y)} - e^{(y)}) \right)$

$e^{(y+1)} = e^{(y)} + \overline{O} L_k^{(y+1)} - w_k^{-(y)}$

End while $L_k^{(p+1)} = L_k^{(J+1)}$

$\tilde{G}_k = \tilde{G}_k \overline{G}_k^p$

Update $\Delta w_k^{-(p+1)}$ based on (13), (14), and (16)

$w_k = \tilde{w}_k + \Delta w_k^{-(p+1)}$,
$\overline{G}_k^{(p+1)} = diag\left\{ \exp(h2\pi \sum_{t=1}^{i} \Delta w_k^{-(p+1)}(t)) \right\}$

End while

Output individual components R_k and IFs w_k

The technique is a sequential optimization method consisting of two loops. The inner loop is responsible for forecasting the intricate envelope, while the outer loop is responsible for extracting individual constituents and Intermediate Frequencies (IFs).

The initial value of the phase error $\bar{G}_k^{(1)} = P$ is established in the outer loop. The complex envelope $L_k^{(1)} = SN_k^p$ and the running total of the residuals $e^{(1)} = 0$ are initialized at the beginning of the inner loop. Finally, the EVCCD model separates the multicomponent signal into an indusial signal in a short time.

3. Results and Discussion

This section presents experimental analyses conducted on both the proposed decomposition algorithm and the existing decomposition algorithm. The performance of each model is compared and evaluated using the multicomponent signal to separate individual component signals. A range of metrics, including Root Mean Square Error (RMSE), Root Mean Absolute Error (RMAE), Mean Square Error (MSE), and Signal-to-Noise Ratio (SNR), are calculated for each model in real-life signals.

The error of the suggested decomposition algorithm is then compared with existing decomposition algorithms such as Resonance-based Signal Decomposition (RSD), Chirplet Signal Decomposition (CSD), Recursive Variational Mode Decomposition algorithm (RVMD), and Improved Empirical Mode Decomposition algorithm (IEMD).

The results offer a comprehensive overview and comparison of these metrics across various models. Table 3 provides specifics about the system design of the suggested model.

Table 3. Analysis of the suggested model's system configuration

Processor	Intel(R) Core(TM) i5-3570 CPU @ 3.40GHz 3.40 GHz
Installed RAM	8.00 GB (7.89 GB usable)
System Type	64-bit operating system, x64-based processor
Pen and Touch	No pen or touch input is available for this display.
Edition	Windows 10 pro
Version	22H2

3.1. Performance Metrics

The proposed EVCCD method for individual component decomposition is evaluated based on several performance metrics. Here are the calculations for each metric:

3.1.1. RMSE

RMSE measures the discrepancy between the expected and observed values. This is calculated by finding the square root of the mean of the squared differences between the expected and observed values.

3.1.2. RMAE

The RMAE measures the difference between the expected and actual values of a signal. The mean of the absolute differences between the predicted and observed values is calculated.

3.1.3. MSE

The Mean Squared Error (MSE) is a measure that determines the average of the squared differences between the predicted and observed values. The calculation entails determining the mean of the squared differences between the anticipated and observed values.

3.1.4. SNR

SNR measures the strength of a signal relative to the noise present in the signal. In this context, it is used to evaluate the quality of the separated component signals.

3.2. Comparative Analysis with Proposed and Existing Method

Using the real-life multicomponent signal, this study proposed the EVCCD method against the existing decomposition method to correctly separate the individual component signal. Figure 2 and Table 4 illustrate the comparison between the proposed EVCCD method and an existing decomposition technique concerning MSE across various SNRs.

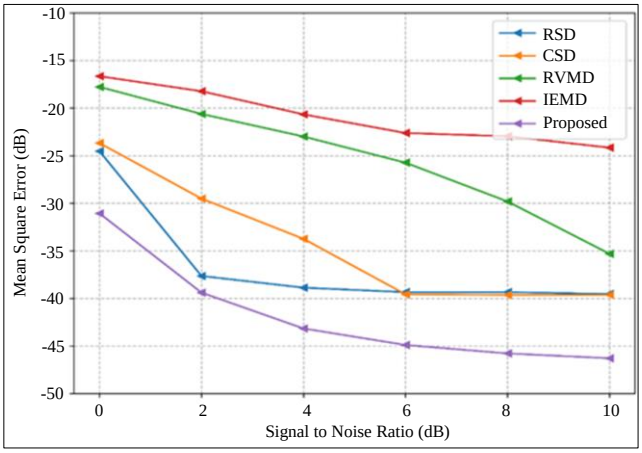

Fig. 2 Analysis of MSE

Comparing the suggested method to the current decomposition method, Figure 2 illustrates a prominent enhancement in MSE reduction. When related to the current procedure, the suggested method performs better. Specifically, the proposed method achieves a 31% reduction in MSE for individual component signals. This improvement is made possible by tackling the sparse regularization problem, a frequent problem in decomposition techniques. When a signal's length is significantly less than its number of non-zero coefficients, the sparse regularization problem occurs.

By addressing this problem, the proposed method can obtain less MSE and improve its performance because the existing decomposition algorithm has some limitations, such as obtaining many loss problems. Figure 3 and Table 5 present a visual representation comparing the proposed EVCCD method with an established decomposition technique regarding RMAE across varying SNRs.

The performance of the suggested method and the current decomposition method for individual component signals is shown in Figure 3 in terms of RMAE reduction. When comparing the suggested method to the current decomposition method, there is a noticeable improvement in RMAE reduction. Specifically, the proposed method achieves a 0.014% reduction in RMAE for individuals.

Table 4. Analysis of MSE with SNR in individual signals

Methods	MSE (SNR) (dB)					
	0	**2**	**4**	**6**	**8**	**10**
RSD	-24.52	-37.64	-38.86	-39.34	-39.34	-39.52
CSD	-23.67	-29.50	-33.73	-39.56	-39.64	-39.62
RVMD	-17.77	-20.61	-22.98	-25.73	-29.81	-35.30
IEMD	-16.65	-18.22	-20.66	-22.61	-22.95	-24.15
Proposed	**-31.06**	**-39.39**	**-43.15**	**-44.89**	**-45.77**	**-46.28**

Table 5. Analysis of RMAE with SNR in the individual signal

Methods	RMAE (SNR) (dB)					
	0	**2**	**4**	**6**	**8**	**10**
RSD	0.088	0.074	0.047	0.042	0.038	0.034
CSD	0.085	0.067	0.038	0.03	0.024	0.025
RVMD	0.061	0.05	0.038	0.03	0.023	0.022
IEMD	0.056	0.048	0.038	0.027	0.019	0.017
Proposed	0.052	0.045	0.035	0.024	0.018	0.013

Table 6. Analysis of RMSE with SNR in individual signal

Methods	RMSE (SNR) (dB)				
	-20	-10	0	10	20
RSD	-13.358	-14.672	-25.255	-25.234	-21.168
CSD	-14.881	-15.96	-25.555	-28.665	-31.421
RVMD	-14.582	-15.818	-29.055	-38.327	-42.655
IEMD	-14.782	-16.058	-30.657	-41.431	-46.131
Proposed	-15.829	-19.942	-36.448	-45.648	-49.49

This improvement is due to the fact that the proposed method can accurately separate individual component signals, while the existing method cannot. Compared to the current strategy, the suggested approach can achieve greater results.

Figure 4 and Table 6 present a graphical comparison between the proposed EVCCD method and an existing decomposition approach regarding RMSE across different SNRs.

The performance of the suggested method and the current decomposition method for individual component signals is shown in Figure 4 in terms of RMSE reduction. When comparing the suggested method to the current decomposition method, there is a noticeable improvement in RMSE decrease. Specifically, the proposed method achieves a 45% reduction in RMSE for individual component signals. This improvement is due to the fact that the proposed method uses STFT to easily identify the TFR and estimate the IF of the signals. In contrast, the existing method has some complexity in generating the TFR.

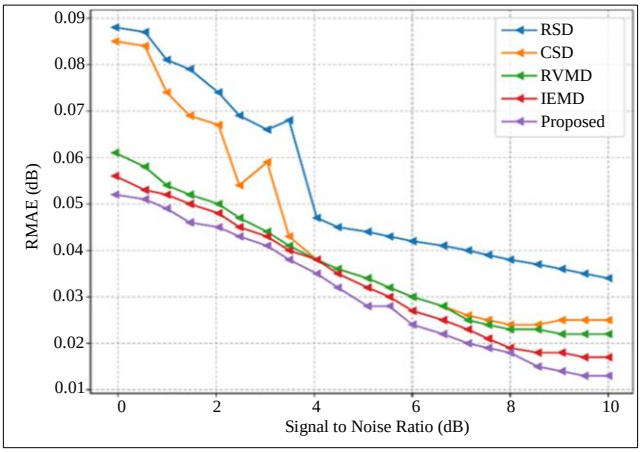

Fig. 3 Analysis of RMAE

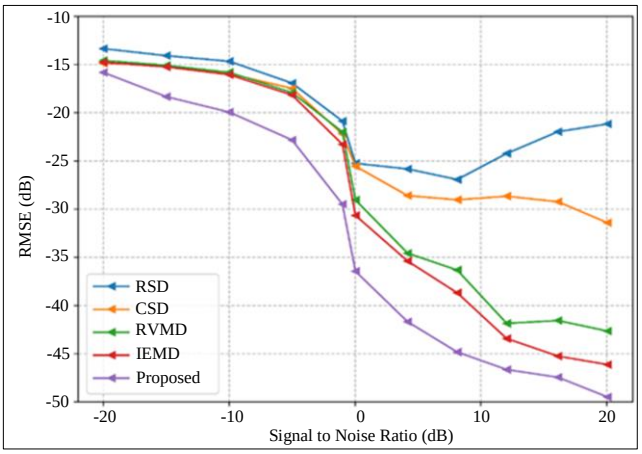

Fig. 4 Analysis of RMSE

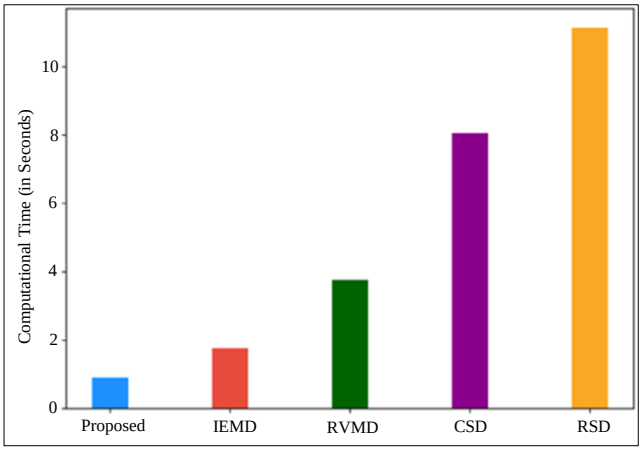

Fig. 5 Analysis of computational time

Figure 5 and Table 7 present a comparison of computational time between the proposed and existing methods. The computing times of the suggested approach and the current method are contrasted in Figure 4. The proposed method can achieve a much lower computational time of just 0.90284% compared to the existing method. This indicates that the suggested approach for dissecting signals into their constituent signals is far quicker and more effective.

Table 7. Comparison between proposed and existing method computational time

Methods	Computational Time
Proposed	0.90282
IEMD	1.76779
RVMD	3.76746
CSD	8.05714
RSD	11.1426

The proposed method mentioned in the table is a signal processing technique that separates individual component signals from a multicomponent incomplete signal. This method is efficient as it requires less time to process the signal than other traditional methods. Figures 6 to 10 present the total result of the suggested approach. Upon further examination of Figures 6 to 10, it becomes evident that the proposed method adeptly and efficiently separates the multicomponent signal.

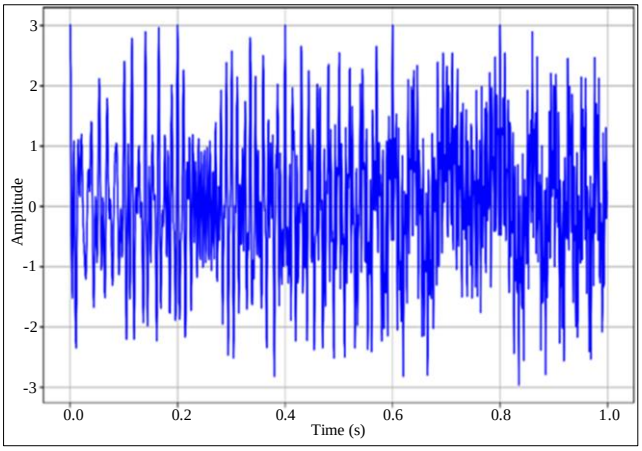

Fig. 6 Original multicomponent signal

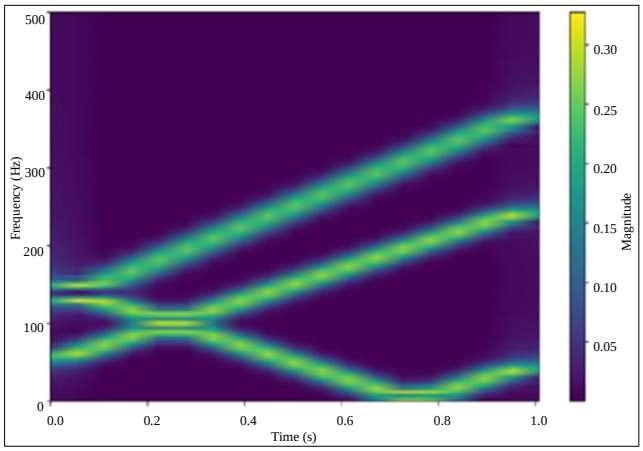

Fig. 7 Time-frequency representation

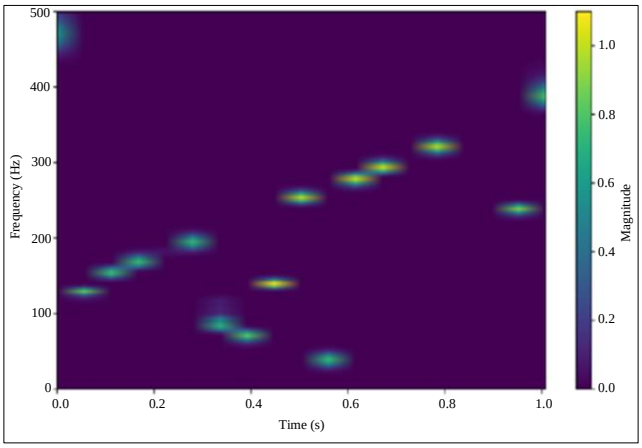

Fig. 8 Reconstructed time-frequency representation

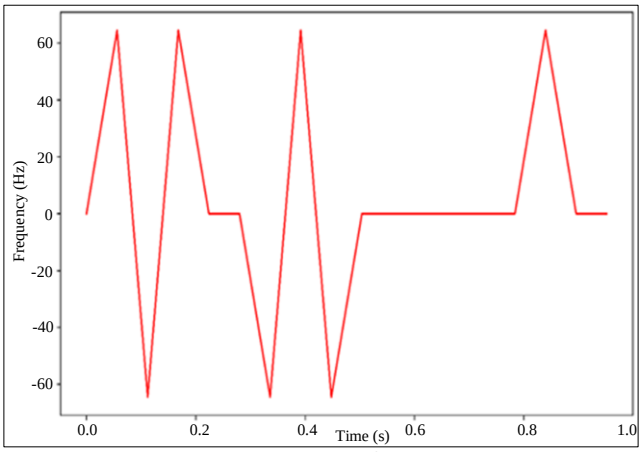

Fig. 9 Instantaneous frequency

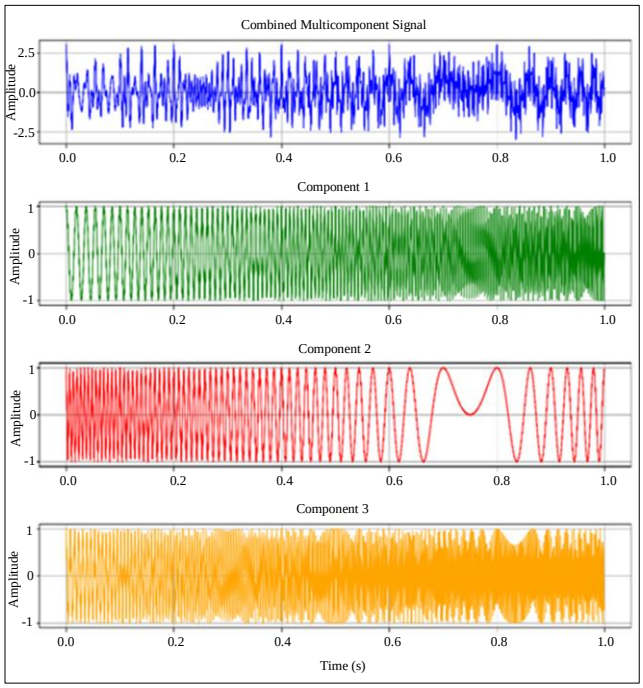

Fig. 10 Multicomponent signal to separate the individual signal

4. Conclusion

This paper introduces the novel EVCCD approach for efficiently decomposing multicomponent incomplete signals. The EVCCD method processes signals by first applying STFT to obtain a time-frequency representation. This representation is then refined using Compressive Sensing, specifically RISTN, to solve a sparse regularization problem. The IF is estimated using the SVMD algorithm. The modelling and experimental findings demonstrate that the proposed EVCCD approach surpasses existing methods in terms of RMSE, MSE, RMAE, and computing time, achieving values of -15.829 dB, -31.062 dB, 0.034 dB, and 0.90282, respectively. The results underscore the potential of the EVCCD approach for signal decomposition and provide a good outlook for future study. Our future goals include enhancing the performance of the EVCCD approach, expanding its applicability to a broader spectrum of signals, and investigating its potential for real-time applications. The goal is to provide a robust and efficient solution for decomposing complex signals, which can benefit various domains, including signal processing, communication systems, and biomedical engineering.

References

[1] Jing Wu et al., "Micro-Doppler Curve Extraction Based on Reassociation Viterbi Algorithm," *IEEE Transactions on Aerospace and Electronic Systems*, vol. 60, no. 4, pp. 4295-4309, 2024. [CrossRef] [Google Scholar] [Publisher Link]

[2] Huan Wang et al., "TFR Reconstruction from Incomplete m-D Signal via Adaptive Hadamard Product Parametrization," *IEEE Geoscience and Remote Sensing Letters*, vol. 20, 2023. [CrossRef] [Google Scholar] [Publisher Link]

[3] Quentin Legros et al., "Instantaneous Frequency and Amplitude Estimation in Multi-Component Signals Using an EM-based Algorithm," *IEEE Transactions on Signal Processing*, vol. 72, pp. 1130-1140, 2024. [CrossRef] [Google Scholar] [Publisher Link]

[4] Yanbo Mai et al., "ISAR Imaging of Target Exhibiting Micro-Motion Components Based on Joint Constraints of Low Rank and Structured Sparsity," *IEEE Transactions on Antennas and Propagation*, vol. 72, no. 5, 2024. [CrossRef] [Google Scholar] [Publisher Link]

[5] Yipeng Ding et al., "Improved Linear Chirplet Transform and Singular Value Decomposition Joint Algorithm for Motion Target Tracking," *IEEE Internet of Things Journal*, vol. 11, no. 8, pp. 13383-13392, 2024. [CrossRef] [Google Scholar] [Publisher Link]

[6] Yuebin Wang et al., "An RFS Time-Frequency Model for Decomposing Chirp Modes with Dynamic Cross, Appearance and Disappearance," *IEEE Transactions on Aerospace and Electronic Systems*, vol. 59, no. 4, pp. 4525-4539, 2023. [CrossRef] [Google Scholar] [Publisher Link]

[7] Vaishali S. Amin, Yimin D. Zhang, and Braham Himed, "Improved Time-Frequency Representation of Multi-Component FM Signals with Compressed Observations," *2020 54th Asilomar Conference on Signals, Systems, and Computers*, Pacific Grove, CA, USA, pp. 1370-1374, 2020. [CrossRef] [Google Scholar] [Publisher Link]

[8] Qiyu Tu et al., "Local Maximum Multisynchrosqueezing Transform and its Application," *Digital Signal Processing*, vol. 140, 2023. [CrossRef] [Google Scholar] [Publisher Link]

[9] Xingxing Jiang et al., "Synchronous Chirp Mode Extraction: A Promising Tool for Fault Diagnosis of Rolling Element Bearings under Varying Speed Conditions," *Chinese Journal of Aeronautics*, vol. 35, no. 1, pp. 348-364, 2022. [CrossRef] [Google Scholar] [Publisher Link]

[10] Jie Huang et al., "Adaptive Multivariate Chirp Mode Decomposition," *Mechanical Systems and Signal Processing*, vol. 186, 2023. [CrossRef] [Google Scholar] [Publisher Link]

[11] Qing Li, "Spatio-Temporal Nonconvex Penalty Adaptive Chirp Mode Decomposition for Signal Decomposition of Cross-Frequency Coupled Sources in Seafloor Dynamic Engineering," *Frontiers in Marine Science*, vol. 9, 2022. [CrossRef] [Google Scholar] [Publisher Link]

[12] Jiakai Ding et al., "Slope Synchronous Chirplet Transform and its Application to Tacho-less Order Tracking of Rotating Machineries," *Mechanical Systems and Signal Processing*, vol. 196, 2023. [CrossRef] [Google Scholar] [Publisher Link]

[13] Hongkang Wu et al., "Multivariate Complex Modulation Model Decomposition and its Application to Gear Fault Diagnosis," *Digital Signal Processing*, vol. 135, 2023. [CrossRef] [Google Scholar] [Publisher Link]

[14] Yun Tao Xu, and Zhi Yong Song, "Multi-Component Signal Separation Using CFAR and DBSCAN Based on Ridge Path Regrouping," *Proceedings of the 2023 International Conference on Frontiers of Artificial Intelligence and Machine Learning*, pp. 14-18, 2023. [CrossRef] [Google Scholar] [Publisher Link]

[15] Yi Li, Weijie Xia, and Shiqi Dong, "Time-Based Multi-Component Irregular FM Micro-Doppler Signals Decomposition via STVMD," *IET Radar, Sonar & Navigation*, vol. 14, no. 10, pp. 1502-1511, 2020. [CrossRef] [Google Scholar] [Publisher Link]

[16] Huan Wang et al., "Decomposition for Multi-Component Micro-Doppler Signal with Incomplete Data," *IEEE Geoscience and Remote Sensing Letters*, vol. 19, 2022. [CrossRef] [Google Scholar] [Publisher Link]

[17] Jie Lu et al., "Non-Sinusoidal Micro-Doppler Estimation Based on Dual-Branch Network," *Remote Sensing*, vol. 14, no. 19, 2022. [CrossRef] [Google Scholar] [Publisher Link]

[18] Xin Huang et al., "Multicomponent Collaborative Time-Frequency State-Space Model for Vibration Signal Decomposition under Nonstationary Conditions," *Measurement Science and Technology*, vol. 35, no. 6, 2024. [CrossRef] [Google Scholar] [Publisher Link]

[19] Jamal Akram et al., "Multi-Component Instantaneous Frequency Estimation Using Signal Decomposition and Time-Frequency Filtering," *Signal, Image and Video Processing*, vol. 14, no. 8, pp. 1663-1670, 2020. [CrossRef] [Google Scholar] [Publisher Link]

[20] Lu Yan et al., "Mechanical Varying Non-Stationary Signal Separation Method Based on Instantaneous Frequency Estimation," *Advances in Mechanical Engineering*, vol. 15, no. 5, 2023. [CrossRef] [Google Scholar] [Publisher Link]

[21] Lei Tang et al., "An Improved Local Maximum Synchrosqueezing Transform with Adaptive Window Width for Instantaneous Frequency Identification of Time-Varying Structures," *Engineering Structures*, vol. 292, 2023. [CrossRef] [Google Scholar] [Publisher Link]